ChemComm

COMMUNICATION

View Article Online
View Journal

Cite this: DOI: 10.1039/d6cc02157c

Received 8th April 2026,
Accepted 28th April 2026

DOI: 10.1039/d6cc02157c

rsc.li/chemcomm

Sodium-metal and strontium-metal nanoparticles

Christian Ritschel,[a] Radian Popescu,[b] Yolita M. Eggeler[b] and Claus Feldmann*[a]

Nanoparticles of zerovalent sodium metal (5 ± 1 nm) and strontium metal (7 ± 3 nm) are synthesized in the liquid phase for the first time. The synthesis is performed in toluene with NaCp or SrI_2 and TMEDA-stabilized [LiNaph] as the reducing agent (TMEDA: *N,N,N′,N′*-tetramethylethylenediamine; [LiNaph]: lithium naphthalenide). Both nanoparticles are crystalline and highly reactive, as exemplarily indicated by the formation of phase-pure alkalides.

The knowledge on metal nanoparticles is the smaller the more basic the respective metal. In particular, this relates to a great number of base metals with electrochemical potentials (E^0) of −1.0 to −2.5 V (taking E^0 of the respective bulk metal as an indicator).[1] The limited knowledge about base-metal nanoparticles can be illustrated by the annual number of publications on selected metal nanoparticles.[2] Thus, more than 5000 publications addressed the synthesis of Au(0) nanoparticles (E^0(bulk-Au) = +1.5 V)[1] in 2025,[2] about 500 publications were related to the synthesis of Co(0) nanoparticles (E^0(bulk-Co) = −0.3 V),[1,2] whereas no report in 2025 addressed the synthesis of, for instance, Ti(0) nanoparticles (E^0(bulk-Ti) = −1.9 V).[1] Current knowledge can be correlated to the synthesis of base-metal nanoparticles, which is the more demanding the higher their reactivity and the smaller their size.[3]

Base-metal nanoparticles have attracted our interest, in general. In recent years, we have developed various methods to prepare base-metal nanoparticles, including microemulsions with liquid ammonia, sodium-driven reduction in liquid ammonia, lithium/sodium pyridinyl-driven reduction in pyridine, and lithium/sodium naphthalide-driven ([LiNaph], [NaNaph]) reduction in THF.[4] In addition to the development of synthetic strategies, base-metal nanoparticles turned out to be useful starting materials for redox reactions with small molecules (O_2, S_8, NH_3, ROH, *etc.*), sterically demanding O–H-/N–H-acidic alcohols/amines or cyclic ethers to obtain new coordination compounds, metal–metal bonding, or cluster compounds.[4d,5] Particularly, the reduction of metal halides by [LiNaph] in THF turned out to be a versatile approach. Thus, we could synthesize all group 3–6 transition metals, all lanthanide metals (La to Lu), Mg and Al with a size of 1–5 nm.[4d] These metals – as bulk metals – have electrochemical potentials in the range of −1.0 to −2.5 V.[1] Sodium and strontium, however, exhibit even more negative electrochemical potentials of −2.7 V and −2.9 V.[1] These highly negative values add further challenges to the synthesis of nanoparticles. First, THF is no longer stable as a solvent. Thus, reductive polymerization of THF is preferred over the reduction of Na^+ or Sr^{2+} in THF.[6] Such behaviour and reaction were already described for the reaction of THF and alkali metals.[7] Moreover, the reduction potential of [LiNaph] in THF was reported to be about −2.3 V, so the reducibility of Na^+/Sr^{2+} with [LiNaph] is questionable anyway.[8]

Aiming at Na(0) and Sr(0) nanoparticles, a modification of our previous synthesis strategy using [LiNaph]-driven reduction in THF was necessary as otherwise THF is either reductively polymerized[6] or naphthalides such as [Sr(naph)(thf)$_2$], containing Sr^{2+} and $[naph]^{2-}$, are formed.[5d] Instead of THF, therefore, we have selected toluene as the solvent, which – due to the absence of any heteroatom – can be expected to be less coordinative and have even higher redox stability. As another difficulty, however, all starting materials – [LiNaph], NaCp,[9] and SrI_2 – are insoluble in toluene (Fig. S1 and S2, SI). From the synthesis of Al(0) nanoparticles,[10] we learned that [LiNaph] becomes soluble in toluene upon coordination to *N,N,N′,N′*-tetramethylethylenediamine (TMEDA) (Fig. 1 and Fig. S3, SI). NaCp and SrI_2, however, remain insoluble in toluene even in the presence of TMEDA.

Due to the aforementioned restrictions regarding the solubility of NaCp and SrI_2 in toluene, both were added here as pure powders. Despite these – at first sight – non-optimal conditions

[a] *Institut für Anorganische Chemie, Karlsruhe Institute of Technology (KIT), Engesserstrasse 15, 76131, Karlsruhe, Germany. E-mail: claus.feldmann@kit.edu; Fax: +49 721 608 47021; Tel: +49 721608 42855*
[b] *Laboratory for Electron Microscopy, Karlsruhe Institute of Technology (KIT) Engesserstrasse 7, D-76131, Karlsruhe, Germany*

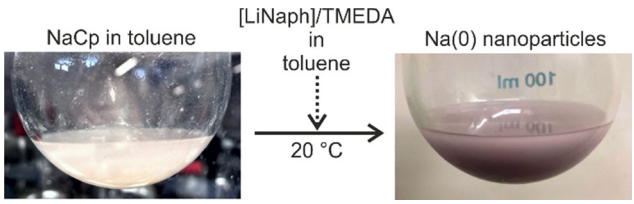

Fig. 1 Scheme illustrating the liquid-phase synthesis of Na(0) with photos of the NaCp precursor in toluene and the as-prepared Na(0) nanoparticles in toluene (see Fig. S3, SI, for the synthesis of Sr(0) nanoparticles).

for nanoparticle preparation, the reduction and nucleation of Na(0) and Sr(0) nanoparticles were nevertheless successful. On the one hand, the dissolution of NaCp and SrI_2 is very slow, whereas the reduction by [LiNaph] after dissolution was very fast (Fig. 1 and Fig. S3, SI). After reduction, moreover, sodium and strontium metals are both highly insoluble in toluene. These effects – fast reduction and low solubility of the as-prepared metals – cause a high supersaturation, promoting the formation of small-sized particles.[11] Successful reduction and nucleation of Na(0) and Sr(0) nanoparticles are indicated by the formation of greyish to black suspensions with slightly reddish (Na) to bluish (Sr) appearance (Fig. 1 and Fig. S3, SI). Whereas the dissolution and reduction of NaCp took some minutes, the dissolution of SrI_2 is very slow and takes about two weeks to complete. Finally, it should be noticed that the as-prepared Sr(0) nanoparticles were very small (1–2 nm) and difficult to separate *via* centrifugation. Here, certain heating (100 °C) was applied to slightly increase the particle size (7 ± 3 nm). Such heating was not necessary for the Na(0) nanoparticles, which were prepared at room temperature.

Subsequent to synthesis, the as-prepared Na(0) and Sr(0) nanoparticles were purified by centrifugation and repeated redispersion/centrifugation in/from THF and toluene to remove remaining naphthalene, TMEDA and LiCp or LiI. Finally, the Na(0)/Sr(0) nanoparticles were either dried in vacuum (10^{-3} mbar) at room temperature to obtain powder samples (Fig. 1 and Fig. S3, SI) or redispersed in toluene or TMEDA to obtain suspensions. It should be noticed that handling of the Na(0) and Sr(0) nanoparticles requires special attention as they are highly pyrophoric and may even explode upon contact with water or other oxidizing agents (Fig. S4 and S5, SI).

Transmission electron microscopy (TEM) is most relevant for characterization and for determining the size, shape, composition, and crystallinity of the as-prepared Na(0) and Sr(0) nanoparticles. However, TEM analysis turned out to be time-consuming and challenging due to the high reactivity of the metal nanoparticles. First of all, contamination with oxygen – predominantly due to traces of water molecules remaining adsorbed on all kinds of surfaces – is a challenge. Although suitable transfer modules were used, the few nanoparticles deposited on a TEM grid were reactive enough to attract all traces of moisture. To address this concern, pre-treatment of TEM grids by heating under vacuum and fast transfer from a glove-box into the TEM device (<30 min) are important. Moreover, the Na(0) and Sr(0) nanoparticles can react with the Lacey-carbon film of the TEM grid under high-energy electron bombardment, which requires precise examination and high experience for TEM characterization.

The as-prepared Na(0) and Sr(0) nanoparticles exhibit a uniform spherical shape with a size in the 5 nm range and a low degree of agglomeration (Fig. 2a, 3a and Fig. S6, S7, SI). Statistical evaluation of about 100 metal nanoparticles in TEM images resulted in a mean particle diameter of 5 ± 1 nm for the Na(0) nanoparticles (Fig. 2b) and 7 ± 3 nm for Sr(0) nanoparticles (Fig. 3b). High-resolution TEM (HRTEM) images confirm the presence and crystallinity of the as-prepared Na(0) and Sr(0) nanoparticles, showing lattice fringes extending through the whole particle (Fig. 2c, 3c and Fig. S6, S7, SI). For the Na(0) nanoparticles, the observed average lattice-fringe distance of 2.9 ± 0.1 Å agrees with that of body-centred cubic (bcc) bulk sodium (d_{110} = 3.03 Å).[12] The two-dimensional Fourier transform (FT) pattern of the nanoparticle in the HRTEM image (Fig. 2c) is in agreement with the calculated diffraction pattern of bcc bulk sodium in the [001]-zone axis (Fig. 2d).[12] In the case of Sr(0) nanoparticles, the observed average lattice-fringe distance of 2.8 ± 0.1 Å corresponds well to the (110) lattice-plane distance (d_{110} = 2.91 Å) of bulk cubic γ-Sr (Fig. 3c).[13] Again, the 2D Fourier transform of a single nanoparticle is in good agreement with the calculated diffraction pattern of bulk cubic γ-Sr (space group: $Im\bar{3}m$; lattice parameter: a = 4.87 Å) in the [001]-zone axis (Fig. 3d).[13] Finally, it should be noticed that the HRTEM images did not show the presence of any oxide species.

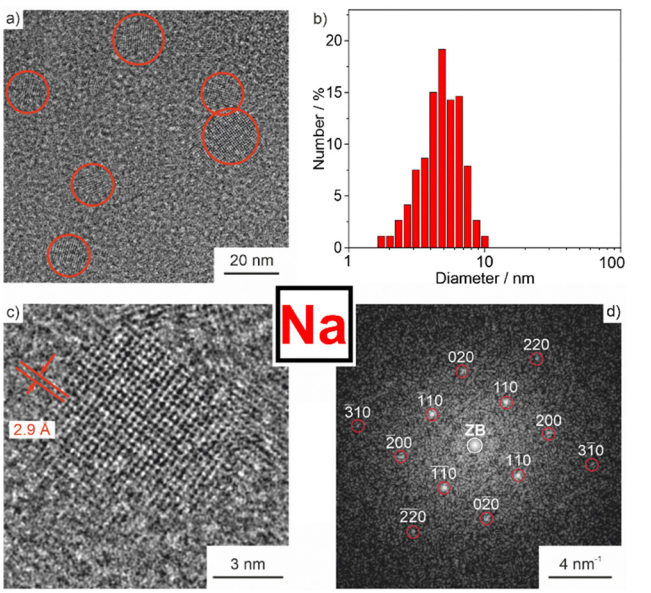

Fig. 2 Electron microscopy of the as-prepared Na(0) nanoparticles: (a) HRTEM overview image showing single nanoparticles (indicated by red dots), (b) size distribution (according to a statistical evaluation of >100 nanoparticles in HRTEM images), (c) HRTEM image of a single nanoparticle with lattice fringes, and (d) FT pattern of a single nanoparticle shown in (c), which agrees with the calculated diffraction pattern of bcc bulk Na (red circles and Miller indices) in the [001] zone axis (zero-order beam, ZB, marked by a white circle).

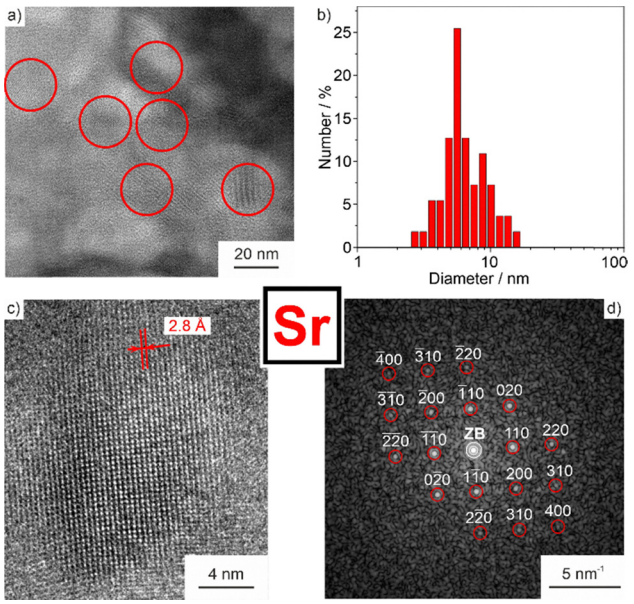

Fig. 3 Electron microscopy of the as-prepared Sr(0) nanoparticles: (a) HRTEM overview image showing single nanoparticles (indicated by red dots), (b) size distribution (according to a statistical evaluation of >60 nanoparticles in HRTEM images), (c) HRTEM image of a single nanoparticle with lattice fringes, and (d) FT pattern of a single nanoparticle shown in (c), which agrees with the calculated diffraction pattern of bulk cubic γ-Sr (red circles and Miller indices) in the [001] zone axis (zero-order beam, ZB, marked by a white circle).

The crystallinity of the Na(0) and Sr(0) nanoparticles was also examined by X-ray powder diffraction (XRD) (Fig. 4). Here, it should be noticed that the metal nanoparticles need to be mortared and diluted with dried quartz powder to enable filling of glass capillaries (0.3 mm in diameter) for XRD analysis. After mortaring, especially low-melting-point sodium (T_{melt}: 98 °C) appears bulk-like and well-crystallized, whereas only broad reflexes indicate the presence of high-melting-point strontium (T_{melt}: 777 °C). Due to the small crystallite size and high X-ray absorption of Sr(0), the scattering intensity is low. Although Na(0) loses its nanoscale size due to mortaring, XRD is nevertheless interesting as only Bragg peaks of the pure metal are observed (Fig. 4). Impurity phases (*e.g.*, halides, oxides, hydroxides, and carbonates) are not observed. Fourier-transform infrared (FT-IR) spectra, recorded by attenuated total reflection (ATR) to examine the particle surface, show only weak vibrations of toluene or naphthalene (1575, 1238, and 734 cm^{-1}) for both the Na(0) and the Sr(0) nanoparticles (Fig. 5). Interestingly, vibrations of the most strongly coordinating chelating ligand TMEDA are not observed.

Elemental (C/H/N) analysis of the Na(0) nanoparticles revealed a surface conditioning composed of 0.6 wt% N, 26.0 wt% C, and 2.5 wt% H. In the case of the Sr(0) nanoparticles, 1.9 wt% N, 40.9 wt% C, and 3.9 wt% H were detected. The N content can be attributed to TMEDA. Moreover, the C : H ratio of 10 : 1 for both metals points to surface functionalization predominantly by toluene (10 : 1) than by naphthalene (15 : 1) in the range of a monolayer. In addition to C/H/N analysis, the thermal properties of the Na(0) and Sr(0) nanoparticles were evaluated by thermogravimetry (TG). For Na(0), first, an increase of mass (62%) is observed (150–400 °C), followed by a mass loss (32%, 500–1000 °C) (Fig. 6a), which can be related to the formation of sodium hyperoxide (NaO_2) (calcd. 59%) followed by the formation of sodium oxide (Na_2O) (calcd. 30%), which, as a strong base, at this temperature reacts with the corundum crucible. In the case of the Sr(0) nanoparticles, certain fluctuation of the mass is observed up to 400 °C, which can be attributed to opposite processes of reaction with O_2 and CO_2 and release of the surface-adhered molecules (Fig. 6b). Above 750 °C, the release of CO_2 (38%) of the intermediately formed $SrCO_3$ occurred (calcd. 30%). Here, the thermal remnant was identified by XRD as a mixture of SrO and $Sr_3Al_2O_6$,[14] of which the latter results from the reaction of SrO with the corundum crucible at high temperature (Fig. S8, SI).

To probe the reactivity of the metal nanoparticles and to verify their suitability for chemical syntheses, we have examined the potential formation of alkalides.[15] Thus, the as-prepared Na(0) nanoparticles were dispersed in toluene and reacted with 2,2,2-cryptand in solution. At −30 °C over 48 h, large amounts of bronze-coloured crystals were obtained (Fig. 7a). XRD with Rietveld refinement indicates these crystals as a pure alkalide with the composition $[Na(2,2,2\text{-cryptand})]^+Na^-$ (Fig. 7b). Such alkalides were only prepared by dissolution of the alkali metal and cryptand in liquid ammonia, as initially introduced by James L. Dye.[15,16] Recently, $[Na(2,2,2\text{-cryptand})]^+Na^-$ was also reported to be synthesized *via* reactive ball milling.[17] The formation of alkalides using metal nanoparticles as the starting

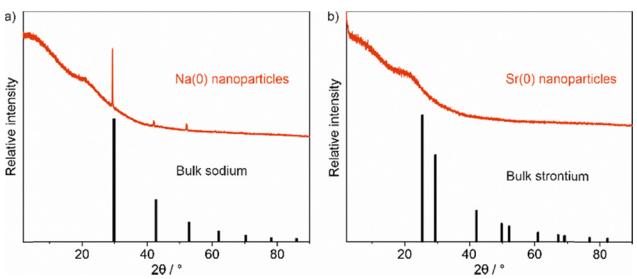

Fig. 4 XRD patterns of (a) Na(0) and (b) Sr(0) nanoparticles with bulk sodium (ICDD No. 01-071-4606) and bulk strontium (ICDD No. 01-089-4045) as references. It must be noticed that filling of glass capillaries (∅: 0.3 mm) required dilution with dried quartz powder and mortaring, which causes fusing of the low-melting-point Na(0) nanoparticles into bulk-like metal.

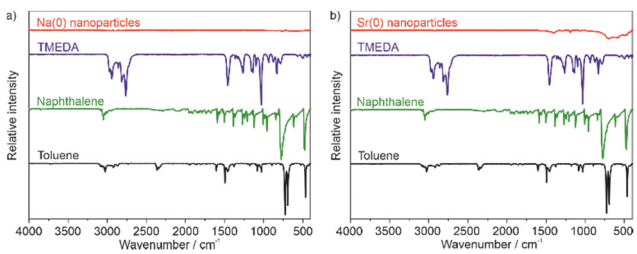

Fig. 5 FT-IR spectra of the as-prepared (a) Na(0) and (b) Sr(0) nanoparticles with the spectra of TMEDA, naphthalene, and toluene as references. All spectra were recorded in ATR mode.

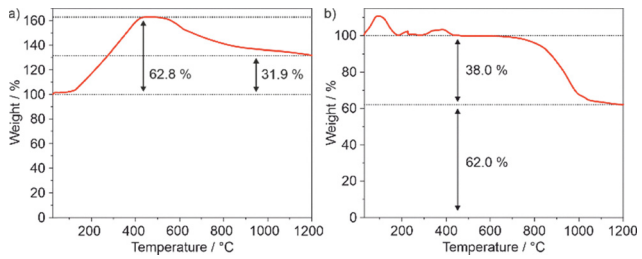

Fig. 6 TG of (a) Na(0) and (b) Sr(0) nanoparticles in air (heating rate: 5 K min^{-1}; crucible material: corundum) (for XRD analysis of the thermal remnant see Fig. S8, SI).

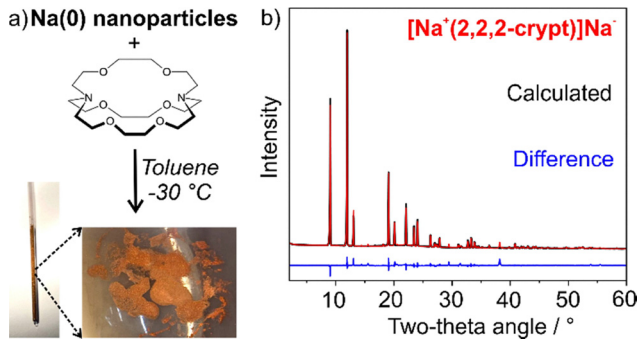

Fig. 7 Synthesis of alkalides with Na(0) nanoparticles: (a) scheme of the reaction with a photo of as-prepared bronze-coloured crystals of $[Na(2,2,2\text{-cryptand})]^+Na^-$; (b) XRD of $[Na(2,2,2\text{-cryptand})]^+Na^-$ (red) with Rietveld refinement (calcd. XRD: black; difference: blue).

material is demonstrated for the first time, and the possibility to perform the reaction in toluene may further expand the repertoire for chemical syntheses.

In conclusion, zerovalent sodium and strontium metal nanoparticles are synthesized in the liquid phase as nanoparticles for the first time. Due to their high reactivity, the synthesis was performed in toluene with TMEDA-stabilized [LiNaph] as the reducing agent and NaCp or SrI_2 as the starting material (TMEDA: *N*,*N*,*N*′,*N*′-tetramethylethylenediamine; [LiNaph]: lithium naphthalenide). This results in colloidally stable suspensions of Na(0) and Sr(0) nanoparticles with a size of 5 ± 1 nm and 7 ± 3 nm. Both nanoparticles are crystalline, showing the structural features of body-centred cubic sodium and cubic γ-strontium. In air, the Na(0) nanoparticles react with O_2 to form the hyperoxide NaO_2 (≥150 °C) as an intermediate and then the oxide Na_2O (≥ 500 °C), whereas the Sr(0) nanoparticles react to produce $SrCO_3$, which decomposes to form SrO (≥750 °C). The reactivity of the metal nanoparticles is further emphasized by direct formation of the pure alkalide $[Na(2,2,2\text{-cryptand})]^+Na^-$ upon reaction of Na(0) nanoparticles with 2,2,2-cryptand in toluene. Despite the first liquid-phase synthesis of Na(0) and Sr(0) nanoparticles, they can also be used as reactive starting materials in non-polar solvents.

Conflicts of interest

The authors declare no conflicts of interest.

Data availability

Additional data regarding experiments and methods can be found in the supporting information (SI) and are available from the authors upon request. Supplementary information: analytical equipment and additional analytic data on the Na(0) and Sr(0) nanoparticles. See DOI: https://doi.org/10.1039/d6cc02157c.

Acknowledgements

The authors acknowledge the Deutsche Forschungsgemeinschaft (DFG) for funding within the Collaborative Research Center 1573 ''4f for Future'' (project A4). C. R. acknowledges the Studienstiftung des deutschen Volkes for a PhD scholarship. The authors gratefully acknowledge Dr. Michael Gamer for providing NaCp.

References

1 N. Wiberg, E. Wiberg and A. F. Holleman, *Anorganische Chemie*, de Gruyter, Berlin, 2017, p. 103, Vol. 1, Annex III/IV.
2 *The American Chemical Society (ACS), Program package Scifinder*, Washington, 2025 (searched on March 10th, 2026).
3 L. Xu, H.-W. Liang, Y. Yang and S.-H. Yu, *Chem. Rev.*, 2018, **118**(7), 3209–3250.
4 (*a*) F. Gyger, P. Bockstaller, D. Gerthsen and C. Feldmann, *Angew. Chem., Int. Ed.*, 2013, **52**, 12443–12447; (*b*) C. Schöttle, P. Bockstaller, D. Gerthsen and C. Feldmann, *Chem. Commun.*, 2014, **50**, 4547–4550; (*c*) A. Egeberg, T. Block, O. Janka, O. Wenzel, D. Gerthsen, R. Pöttgen and C. Feldmann, *Small*, 2019, **15**, 1902321; (*d*) D. Bartenbach, O. Wenzel, R. Popescu, L.-P. Faden, A. Reiß, M. Kaiser, A. Zimina, J.-D. Grunwaldt, D. Gerthsen and C. Feldmann, *Angew. Chem., Int. Ed.*, 2021, **60**, 17373–17377.
5 (*a*) L.-P. Faden, C. Donsbach, R. Popescu, L. Bayarjargal, Y. M. Eggeler, B. Winkler and C. Feldmann, *J. Mater. Chem. C*, 2025, **13**, 23269–23279; (*b*) L.-P. Faden, A. Reiß, R. Popescu, C. Donsbach, J. Göttlicher, T. Vitova, D. Gerthsen and C. Feldmann, *Inorg. Chem.*, 2024, **63**, 1020–1034; (*c*) A. Reiß, A. Appenzeller, J. Baur, J. Wenzel, R. Popescu, K. Beuthert, S. Dehnen, Y. M. Eggeler, F. Breher, W. Klopper and C. Feldmann, *Small*, 2025, **21**, 2503498; (*d*) C. Ritschel, A. Appenzeller, R. Popescu, C. Donsbach, J. O. Wenzel, F. Breher, Y. M. Eggeler, W. Klopper and C. Feldmann, *Angew. Chem., Int. Ed.*, 2025, **64**, e202515995.
6 A. Reiß, C. Donsbach and C. Feldmann, *Dalton Trans.*, 2021, **50**, 16343–16352.
7 J. Bhattacharjee, A. Harinath, H. P. Nayek, A. Sarkar and T. K. Panda, *Chem. – Eur. J.*, 2017, **23**, 9319–9331.
8 N. G. Connelly and W. E. Geiger, *Chem. Rev.*, 1996, **96**, 877–910.
9 T. K. Panda, M. T. Gamer and P. W. Roesky, *Organometallics*, 2003, **22**, 877–878.
10 S. Riegsinger, R. Popescu, D. Gerthsen and C. Feldmann, *Chem. Mater.*, 2024, **36**, 10496–10503.
11 V. K. LaMer and R. H. Dinegar, *J. Am. Chem. Soc.*, 1950, **72**, 4847–4854.
12 E. Aruja and H. Perlitz, *Z. Kristallogr.*, 1939, **100**, 195–200.
13 R. G. Hirst, A. J. King and F. A. Kanda, *J. Phys. Chem.*, 1956, **60**, 302–304.
14 B. C. Chakoumakos, G. A. Lager and J. A. Fernandez-Baca, *Acta Crystallogr., Sect. C: Cryst. Struct. Commun.*, 1992, **48**, 414–419.
15 J. L. Dye, *Acc. Chem. Res.*, 2009, **42**, 1564–1572.
16 F. J. Tehan, B. L. Barnett and J. L. Dye, *J. Am. Chem. Soc.*, 1974, **96**, 7203.
17 N. M. Davison, J. M. Hemingway, C. Wills, T. Stolar, P. G. Waddell, C. M. Dixon, L. Barron, J. Dawson and E. Lu, *Inorg. Chem.*, 2024, **63**, 15247–15258.